

# Fisher matrix predictions for detecting the cosmological 21 cm signal with the Ooty Wide Field Array (OWFA)

Somnath Bharadwaj<sup>1,2\*</sup>, Anjan Kumar Sarkar<sup>2†</sup> and Sk. Saiyad Ali<sup>3‡</sup>

<sup>1</sup> *Department of Physics, IIT Kharagpur, 721302, India*

<sup>2</sup> *Centre for Theoretical Studies, IIT Kharagpur, 721302, India*

<sup>3</sup> *Department of Physics, Jadavpur University, Kolkata 700032, India*

**Abstract.** We have used the Fisher matrix formalism to quantify the prospects of detecting the  $z = 3.35$  redshifted 21-cm HI power spectrum with the upcoming radio-interferometric array OWFA. OWFA’s frequency and baseline coverage spans comoving Fourier modes in the range  $1.8 \times 10^{-2} \leq k \leq 2.7 \text{ Mpc}^{-1}$ . The OWFA HI signal, however, is predominantly from the range  $k \leq 0.2 \text{ Mpc}^{-1}$ . The larger modes, though abundant, do not contribute much to the HI signal. In this work we have focused on combining the entire signal to achieve a detection. We find that a  $5 - \sigma$  detection of  $A_{HI}$  is possible with  $\sim 150$  hr of observations, here  $A_{HI}^2$  is the amplitude of the HI power spectrum. We have also carried out a joint analysis for  $A_{HI}$  and  $\beta$  the redshift space distortion parameter. Our study shows that OWFA is very sensitive to the amplitude of the HI power spectrum. However, the anisotropic distribution of the  $\mathbf{k}$  modes does not make it very suitable for measuring  $\beta$ .

*Key words:* cosmology: large scale structure of universe - intergalactic medium - diffuse radiation

## 1. Introduction

Work is currently in progress to upgrade the cylindrical Ooty Radio Telescope (ORT<sup>1</sup>) so that it functions as a linear interferometric array the Ooty Wide Field Array (OWFA; Prasad & Subrahmanya 2011a,b; Ram Marthi

---

\*Email:somnath@phy.iitkgp.ernet.in

†Email:anjan@cts.iitkgp.ernet.in

‡Email:saiyad@phys.jdvu.ac.in

<sup>1</sup><http://rac.ncra.tifr.res.in/>

& Chengalur 2014). This telescope operates at a nominal frequency of  $\nu_o = 326.5$  MHz which corresponds to the neutral hydrogen (HI) 1,420 MHz radiation from a redshift  $z = 3.35$ . Observations of the fluctuations in the contribution from the HI to the diffuse background radiation are a very interesting probe of the large-scale structures in the high- $z$  universe (Bharadwaj, Nath & Sethi 2001, Bharadwaj, & Sethi 2001). In addition to the power spectrum (Bharadwaj & Pandey 2003, Bharadwaj & Srikant 2004) this is also a sensitive probe of the bispectrum (Ali, Bharadwaj and Pandey 2006, Guha Sarkar & Hazra 2013). There has been a continued, growing interest towards the detection of the 21 cm signal from the lower redshifts ( $0 < z < 4$ ) to probe the post-reionization era (Chang et al. 2008; Visbal et al. 2009; Bharadwaj et al. 2009; Wyithe & Loeb 2009; Bagla, Khandai & Datta 2010; Seo et al. 2010; Mao 2012; Ansari et al. 2012; Bull et al. 2014; Villaescusa-Navarro et al. 2014). Recently, Ali & Bharadwaj (2014) (henceforth, Paper I) have studied the prospects for detecting the HI signal from redshift  $z = 3.35$  using OWFA. The OWFA provides an unique opportunity to study the large scale structures at  $z = 3.35$ .

A number of similar upcoming packed radio interferometer (CHIME<sup>2</sup>, Bandura et al. 2014; BAOBAB<sup>3</sup> and the KZN array<sup>4</sup>) have been proposed to probe the expansion history of the low-redshift universe ( $z \leq 2.55$ ) with an unprecedented precision using BAO measurements from the large-scale HI fluctuations. Even more innovative designs are being planned for the future low frequency telescope SKA<sup>5</sup>. This promises to yield highly significant measurements of the HI power spectrum over a large redshift range spanning nearly the entire post-reionization era ( $z < 6$ ). However, the detection of the faint 21 cm HI signal ( $\sim 1$  mK) is extremely challenging due to the presence of different astrophysical foregrounds. The foregrounds are four to five orders of magnitude brighter than the post-reionization HI signal (Ghosh et al. 2011a, 2011b).

In this paper, we have considered the visibility correlation (Bharadwaj, & Sethi 2001, Bharadwaj, & Ali 2005) which essentially is the data covariance matrix that is necessary to calculate the Fisher matrix. We have employed the Fisher matrix technique to predict the expected signal-to-noise ratios (SNR) for detecting the HI signal. In our analysis we have assumed that the HI traces the total matter with a linear bias, and the matter power spectrum is precisely as predicted by the standard LCDM model with the parameter values mentioned later. The HI power spectrum is then completely specified by two parameters  $A_{HI}$ , which sets the overall amplitude of the power

---

<sup>2</sup><http://chime.phas.ubc.ca/>

<sup>3</sup><http://bao.berkeley.edu/>

<sup>4</sup>A compacted array of 1225 dishes with diameter 5m each, based on BAOBAB and sited in South Africa

<sup>5</sup><http://www.skatelescope.org/>

spectrum, and  $\beta$  the redshift distortion parameter. The parameter  $A_{HI}$  here is the product of the mean neutral hydrogen fraction ( $\bar{x}_{HI}$ ) and the linear bias parameter ( $b_{HI}$ ). For a detection, we focus on measuring the amplitude  $A_{HI}$ , marginalizing over  $\beta$ . We also consider the joint estimation of  $A_{HI}$  and  $\beta$ . Our entire analysis is based on the assumption that the visibility data contains only the signal and the noise, and the foregrounds and radio-frequency interference have been completely removed from the data.

The BAO feature is within the baseline range covered by OWFA (Paper I). However, the frequency coverage ( $\sim 30$  MHz) is rather small. Further, for the present analysis we have only considered observations in a single field of view. All of these result in having very few Fourier modes across the  $k$  range relevant for the BAO, and we do not consider this here.

The rest of the paper is organized as follows. Section 2 briefly discusses some relevant system parameters for OWFA. In Section 3, we present the theoretical model for calculating the signal and noise covariance, and predict their respective contributions. Here we also estimate the range of  $k$ -modes which are probed by the OWFA. In Section 4 we use the Fisher matrix analysis to make predictions for the SNR as a function of the observing time. Finally, we present summary and conclusions in Section 5.

In this paper, we have used the (Planck + WMAP) best-fit  $\Lambda$ CDM cosmology with cosmological parameters (Ade et al. 2013):  $\Omega_m = 0.318$ ,  $\Omega_b h^2 = 0.022$ ,  $\Omega_\Lambda = 0.682$ ,  $n_s = 0.961$ ,  $\sigma_8 = 0.834$ ,  $h = 0.67$ . We have used the matter transfer function from the fitting formula of Eisenstein & Hu (1998) incorporating the effect of baryonic features.

## 2. Telescope parameters

The ORT is a 530 m long and 30 m wide parabolic cylindrical reflector placed in the north-south direction on a hill with the same slope as the latitude ( $11^\circ$ ) of the station (Swarup et al. 1971; Sarma et al. 1975). It thus becomes possible to observe the same part of the sky by rotating the parabolic cylinder along its long axis. The telescope has 1056 half-wavelength ( $0.5\lambda_0 \approx 0.5$  m) dipoles placed nearly end to end along the focal line of the cylinder. Work is underway to implement electronics that combines the digitized signal from every  $N_d$  successive dipoles so that we have a linear array of  $N_A$  antennas located along the length of the cylinder. The OWFA will, at present, have the ability to operate in two different modes one with  $N_d = 24$  and another with  $N_d = 4$ , referred to as Phase I and Phase II respectively. For our theoretical analysis we have also considered two hypothetical (possibly future) upgrades Phases III and IV with  $N_d = 2$  and  $N_d = 1$  respectively. Table 1 summarizes various parameters for different phases of the array. The individual antennas get more compact, and the field of view increases from Phase I to IV. The

**Table 1.** System parameters for Phases I, II, III and IV of the OWFA .

Parameter	Phase I	Phase II	Phase III	Phase IV
No. of antennas ( $N_A$ )	40	264	528	1056
No. of dipoles $N_d$	24	4	2	1
Aperture area ( $b \times d$ )	30 m $\times$ 11.5 m	30 m $\times$ 1.92 m	30 m $\times$ 0.96 m	30 m $\times$ 0.48 m
Field of View (FoV)	1.75° $\times$ 4.6°	1.75° $\times$ 27.4°	1.75° $\times$ 54.8°	1.75° $\times$ 109.6°
Smallest baseline ( $d_{min}$ )	11.5 m	1.9 m	0.96 m	0.48 m
Largest baseline ( $d_{max}$ )	448.5 m	505.0 m	506.0 m	506.5 m
Total band- width (B)	18 MHz	30 MHz	60 MHz	120 MHz
Single Visibility rms. noise ( $\sigma$ )	1.12 Jy	6.69 Jy	13.38 Jy	26.76 Jy

number of antennas and the frequency bandwidth also increases from Phase I to IV.

For any phase, each antenna has a rectangular aperture of dimensions  $b \times d$ , and is distributed at an interval  $\mathbf{d} = d\hat{\mathbf{i}}$  along the length of the cylinder. The value of  $b$ (= 30m), which corresponds to the width of the parabolic reflector, remains fixed for all the phases. The value of  $d$  varies for the different phases (Table 1 ). The baseline  $\mathbf{U}$  quantifies the antenna pair separation projected perpendicular to the line of sight measured in the units of the observing wavelength  $\lambda$ . Assuming observations vertically overhead, we have the baselines

$$\mathbf{U}_a = a \frac{\mathbf{d}}{\lambda} \quad (1 \leq a \leq N_A - 1). \quad (1)$$

In reality  $\mathbf{U}_1, \mathbf{U}_2, \dots$  vary across the observing bandwidth as frequency changes. However, for the present purpose of the paper we keep  $\mathbf{U}_a$  fixed at the value corresponding to the nominal frequency.

A schematic view of the OWFA array layout is presented in Paper I. The OWFA has a significant number of redundant baselines. For any baseline  $\mathbf{U}_a$  we have  $M_a = (N_A - a)$  times sampling redundancy of the baseline.

### 3. OWFA visibility covariance and the Fisher matrix

The OWFA measures visibilities  $\mathcal{V}(\mathbf{U}_a, \nu_m)$  at a finite number of baselines  $\mathbf{U}_a$  and frequency channels  $\nu_m$  with frequency channel width  $\Delta\nu_c$  spanning a frequency bandwidth  $B$ . The measured visibilities can be expressed as a combination of the HI signal and the noise

$$\mathcal{V}(\mathbf{U}_a, \nu_m) = \mathcal{S}(\mathbf{U}_a, \nu_m) + \mathcal{N}(\mathbf{U}_a, \nu_m) \quad (2)$$

assuming that the foregrounds have been removed. The correlation expected between the HI signal at two different baselines and frequencies can be calculated (Paper I and references therein) using

$$\begin{aligned} \langle \mathcal{S}(\mathbf{U}_a, \nu_n) \mathcal{S}^*(\mathbf{U}_b, \nu_m) \rangle &= \left( \frac{2k_B}{\lambda^2} \right)^2 \int d^2U' \tilde{A}(\mathbf{U}_a - \mathbf{U}') \tilde{A}^*(\mathbf{U}_b - \mathbf{U}') \\ &\times \frac{1}{2\pi r_\nu^2} \int dk_\parallel \cos(k_\parallel r'_\nu \Delta\nu) P_{\text{HI}}\left(\frac{2\pi\mathbf{U}'}{r_\nu}, k_\parallel\right) \end{aligned} \quad (3)$$

where  $P_{\text{HI}}(\mathbf{k}_\perp, k_\parallel)$  is the power spectrum of the 21-cm brightness temperature fluctuation in redshift space,  $\left(\frac{2k_B}{\lambda^2}\right)$  is the conversion from brightness temperature to specific intensity,  $r_\nu$  is the comoving distance from the observer to the region where the HI radiation originated,  $r'_\nu = dr/d\nu$  is the radial conversion factor from frequency interval to comoving separation ( $r_\nu = 6.85$  Gpc and  $r'_\nu = 11.5$  Mpc MHz<sup>-1</sup> for OWFA),  $\Delta\nu = \nu_m - \nu_n$  and  $\tilde{A}(\mathbf{U})$  is the Fourier transform of the OWFA primary beam pattern.

The real and imaginary parts of the noise  $\mathcal{N}(\mathbf{U}_a, \nu_n)$  both have equal variance  $\sigma^2$  with

$$\sigma = \frac{\sqrt{2}k_B T_{sys}}{\eta A \sqrt{\Delta\nu_c t}} \quad (4)$$

where  $T_{sys}$  is the system Temperature,  $\eta$  and  $A = b \times d$  are respectively the efficiency and the geometrical area of the antenna aperture and  $t$  is the observing time. We have used the values  $T_{sys} = 150$  K,  $\eta = 0.6$  and  $\Delta\nu_c = 0.1$  MHz which are the same as in Paper I.

The noise in the visibilities measured at different baselines and frequency channels are uncorrelated. We then have

$$\langle \mathcal{N}(\mathbf{U}_a, \nu_n) \mathcal{N}^*(\mathbf{U}_b, \nu_m) \rangle = \delta_{a,b} \delta_{n,m} 2\sigma^2. \quad (5)$$

Earlier studies (Paper I) have shown that for a fixed baseline ( $U_a = U_b$ ) the HI signal (eq. 3) is correlated out to frequency separations  $|\nu_n - \nu_m| \sim 0.5$  MHz which spans several frequency channels. This implies that the data covariance matrix  $\langle \mathcal{V}(\mathbf{U}_a, \nu_n) \mathcal{V}^*(\mathbf{U}_a, \nu_m) \rangle$  has considerable off-diagonal terms, a feature that is not very convenient for the Fisher matrix analysis.

For the Fisher Matrix analysis it is convenient to use the delay channels  $\tau_m$  (Morales 2005) instead of the frequency channels  $\nu_c$ . We define

$$v(\mathbf{U}_a, \tau_m) = \Delta\nu_c \sum_n e^{2\pi i \tau_m (\nu_n - \nu_0)} \mathcal{V}(\mathbf{U}_a, \nu_n) \quad (6)$$

where  $N_c$  is the number of frequency channels,  $B = N_c \Delta\nu_c$  and

$$\tau_m = \frac{m}{B} \quad \frac{-N_c}{2} < m \leq \frac{N_c}{2}.$$

The covariance matrix  $\langle v(\mathbf{U}_a, \tau_m) v^*(\mathbf{U}_b, \tau_n) \rangle$  is zero if  $n \neq m$ , and we need only consider the diagonal terms  $n = m$ . Defining  $C_{ab}(m) = \langle v(\mathbf{U}_a, \tau_m) v^*(\mathbf{U}_b, \tau_m) \rangle$  we have

$$\begin{aligned} C_{ab}(m) &= \frac{B}{r_\nu^2 r'_\nu} \left( \frac{2k_B}{\lambda^2} \right)^2 \int d^2 U' \tilde{A}(\mathbf{U}_a - \mathbf{U}') \tilde{A}^*(\mathbf{U}_b - \mathbf{U}') P_{\text{HI}} \left( \frac{2\pi \mathbf{U}'}{r_\nu}, \frac{2\pi \tau_m}{r'_\nu} \right) \\ &+ \delta_{a,b} 2 \Delta\nu_c B \frac{\sigma^2}{(N_A - a)}. \end{aligned} \quad (7)$$

The factor  $(N_A - a)^{-1}$  in the noise contribution accounts for the redundancy in the baseline distribution. The functions  $\tilde{A}(\mathbf{U}_a - \mathbf{U}')$  and  $\tilde{A}^*(\mathbf{U}_b - \mathbf{U}')$  have an overlap only if  $a = b$  or  $a = b \pm 1$  (Paper I). The visibilities at two baselines  $\mathbf{U}_a$  and  $\mathbf{U}_b$  are uncorrelated ( $C_{ab}(m) = 0$ ) if  $|a - b| > 1$  *ie.* the visibility at a particular baseline  $\mathbf{U}_a$  is only correlated with the other visibility measurements at the same baseline or the adjacent baselines  $\mathbf{U}_{a \pm 1}$ . Thus, for a fixed  $m$ ,  $C_{ab}(m)$  is a symmetric, tridiagonal matrix. Further, the noise only contributes to the diagonal terms, and it does not figure in the off-diagonal terms.

We use the data covariance  $C_{ab}(m)$  to calculate the Fisher Matrix using

$$F_{\alpha\beta} = \frac{1}{2} \sum_m C_{ab}^{-1}(m) [C_{bc}(m)]_{,\alpha} C_{cd}^{-1}(m) [C_{da}(m)]_{,\beta} \quad (8)$$

where the indices  $a, b, c, d$  are to be summed over all baselines, and  $\alpha, \beta$  refer to the various parameters which are to be estimated from the OWFA data.

It is possible to get further insight into the cosmological information contained in the data covariance  $C_{ab}(m)$  by considering large baselines  $U_a \gg d/\lambda$  where it is reasonable to assume that the function  $\tilde{A}(\mathbf{U}_a - \mathbf{U}') \tilde{A}^*(\mathbf{U}_b - \mathbf{U}')$  in eq. (7) falls sharply in comparison to the slowly changing HI power spectrum as  $\mathbf{U}'$  is varied. The integral in equation eq. (7) can then be approximated as

$$\approx P_{\text{HI}}(\mathbf{k}) \int d^2 U' \tilde{A}(\mathbf{U}_a - \mathbf{U}') \tilde{A}^*(\mathbf{U}_b - \mathbf{U}') \quad (9)$$

where

$$\mathbf{k} \equiv (\mathbf{k}_\perp, k_\parallel) \equiv (\pi[\mathbf{U}_a + \mathbf{U}_b]/r_\nu, 2\pi\tau_m/r'_\nu). \quad (10)$$

The integral in eq. (9) can be evaluated analytically, and we have the approximate formula

$$C_{ab}(m) = B \left[ \frac{(2k_B)^2(4\delta_{a,b} + \delta_{a,b\pm 1})}{9\lambda^2 b d r_\nu^2 r'_\nu} P_{\text{HI}}(\mathbf{k}) + \frac{\delta_{a,b} 2 \Delta\nu_c \sigma^2}{(N_A - a)} \right]. \quad (11)$$

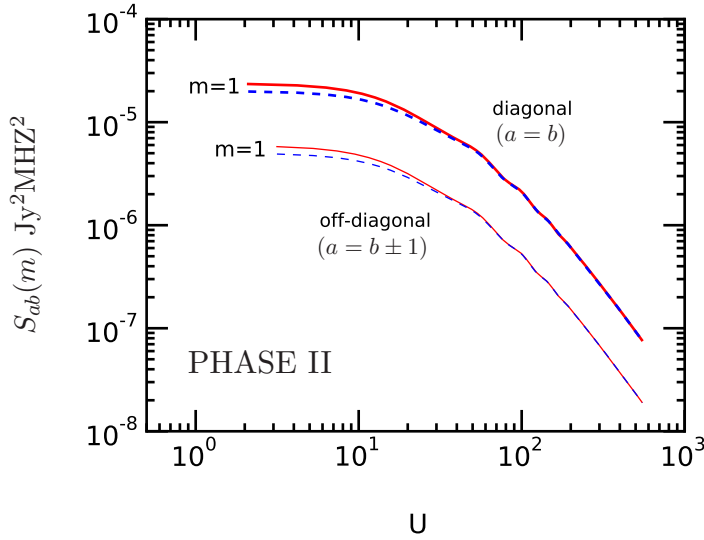


**Figure 1.** This shows the signal contribution to the covariance matrix  $C_{ab}(m)$  for  $m = 1$  calculated using eq. (7) (solid curves) and the approximate formula eq. (11) (dashed curves).

Figure 1 shows a comparison of the signal contribution to the covariance matrix calculated using eq. (7) and the approximate formula eq. (11). We find that the results are in reasonably good agreement over the entire  $U$  range for  $m = 1$ . The agreement is better at large baselines  $U \geq 30$  where the two curves are nearly undistinguishable. The results are indistinguishable for the entire  $U$  range for  $m > 1$  which has not been shown here. Although we have used the approximate equation (eq. 11) to interpret  $C_{ab}(m)$  in the subsequent discussion, we have used eq. (7) to compute  $C_{ab}(m)$  throughout the entire analysis.

Returning to eq. (11), first, the signal contribution to the diagonal terms is found to be 4 times larger than the off-diagonal terms. Next, we see that each non-zero element of the covariance matrix  $C_{ab}(m)$  corresponds to the HI power spectrum at a particular comoving Fourier mode  $\mathbf{k}$  given by eq. (10).

**Table 2.** The  $k_{\perp}$  and  $k_{\parallel}$  range that will be probed by the different Phases of OWFA.

Mpc <sup>-1</sup>	Phase I	Phase II	Phase III	Phase IV
$k_{\perp}[min]$	$1.1 \times 10^{-2}$	$1.9 \times 10^{-3}$	$9.5 \times 10^{-4}$	$4.8 \times 10^{-4}$
$k_{\perp}[max]$	$4.8 \times 10^{-1}$	$5.0 \times 10^{-1}$	$5.1 \times 10^{-1}$	$5.1 \times 10^{-1}$
$k_{\parallel}[min]$	$3.0 \times 10^{-2}$	$1.8 \times 10^{-2}$	$9.1 \times 10^{-3}$	$4.6 \times 10^{-3}$
$k_{\parallel}[max]$	2.73	2.73	2.73	2.73

Each delay channel  $\tau_m$  corresponds to a  $k_{\parallel m} = 2\pi\tau_m/r'_{\nu}$  which spans the values

$$k_{\parallel m} = m \left( \frac{2\pi}{Br'_{\nu}} \right) \quad \frac{-N_c}{2} < m \leq \frac{N_c}{2}. \quad (12)$$

For a fixed  $\tau_m$ , the diagonal terms of  $C_{ab}(m)$  with  $\mathbf{U}_a = \mathbf{U}_b$  correspond to  $k_{\perp a} = 2\pi U_a/r_{\nu}$  which spans the values

$$k_{\perp a} = a \left( \frac{2\pi d}{\lambda r_{\nu}} \right) \quad 1 \leq a \leq N_A - 1, \quad (13)$$

and the off-diagonal terms of  $C_{ab}(m)$  with  $\mathbf{U}_b = \mathbf{U}_{a+1}$  correspond to  $k_{\perp a} = \pi[U_a + U_b]/r_{\nu}$  which spans the values

$$k_{\perp a} = (a \pm 0.5) \left( \frac{2\pi d}{\lambda r_{\nu}} \right) \quad 1 \leq a \leq N_A - 2, \quad (14)$$

We see that the  $k_{\perp}$  value probed by any off-diagonal term is located mid-way between the  $k_{\perp}$  values probed by the two nearest diagonal terms. Considering both the diagonal and the off-diagonal terms, we find that the different  $k_{\perp}$  values that will be probed by OWFA are located at an interval of  $\Delta k_{\perp} = \pi d/(\lambda r_{\nu})$ .

In addition to the HI signal and the noise considered in this paper, the OWFA visibilities will also contain a foreground contribution. For the purpose of this work we make the simplifying assumption that the foregrounds are constant across different frequency channels, and hence they only contribute to the  $k_{\parallel} = 0$  mode. In reality the foreground contamination will possibly extend to other modes also. However, in this work we make the most optimistic assumption that the foregrounds will be restricted to the  $k_{\parallel} = 0$  mode and we have excluded this in the subsequent analysis. Table 2 shows the  $k_{\perp}, k_{\parallel}$  range that will be probed by the different Phases of OWFA. We see that for all the phases (except Phase I) the minimum value of  $k_{\parallel}$  is approximately 10 times larger than the corresponding  $k_{\perp}[min]$ . The sampling along  $k_{\parallel}$ , which is decided by  $1/B$ , has a spacing  $\Delta k_{\parallel} = k_{\parallel}[min]$  which also is  $\sim 5$  times larger than  $\Delta k_{\perp} = k_{\perp}[min]/2$  which is decided by



the antenna spacing  $d$ . The maximum  $k_{\parallel}$  values also are approximately 4 larger than the corresponding  $k_{\perp}[max]$ . It is thus clear that the sampling in  $k_{\perp}$  is quite different from the  $k_{\parallel}$  sampling, and the  $k_{\parallel}$  values are several times larger than the  $k_{\perp}$  values. This disparity in the  $k_{\parallel}$  and  $k_{\perp}$  coverage and sampling poses a problem for using OWFA to quantify redshift space distortion. We shall return to this in Section 5 where we discuss the results of our analysis.

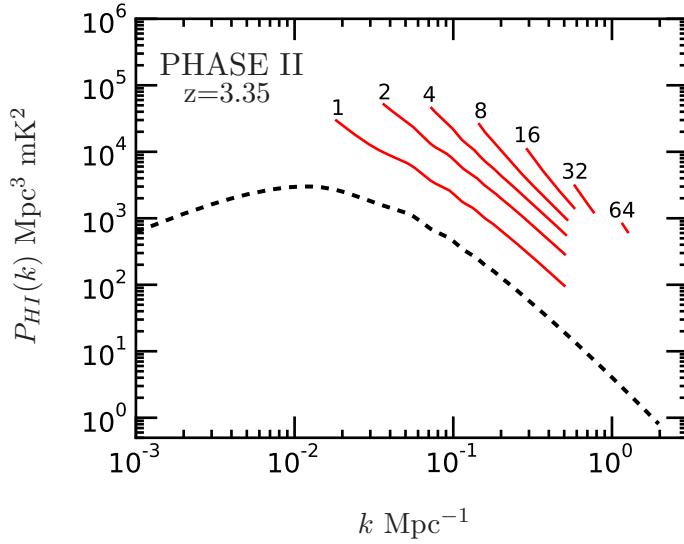


**Figure 2.** The  $k$  range that will be probed by  $C_{ab}(m)$  for different values of  $m$ . The curves for different  $m$  have been arbitrarily displaced vertically to make them distinguishable. For reference, we have also shown the expected 21-cm brightness temperature fluctuation  $P_{HI}(k)$  (dashed curve) where  $P_{HI}(k) \equiv P_{HI}(k, \mu = 0)$  is the  $z = 3.35$  HI 21-cm brightness temperature power spectrum (eq. 15).

Figure 2 shows the  $k = |\mathbf{k}| = \sqrt{k_{\parallel}^2 + k_{\perp}^2}$  range that will be probed by  $C_{ab}(m)$  for different values of  $m$ . We see that the range  $k \sim k_{\parallel}[min]$  to  $k \sim k_{\perp}[max]$  is probed for  $m = 1$ . The  $k$  range shifts to larger  $k$  values as  $m$  is increased, and the entire  $k$  range lies beyond  $1 \text{ Mpc}^{-1}$  for  $m \geq 64$ . Figure 3 shows a histogram of all the different  $k$  modes that will be probed by OWFA Phase II. We expect the number of modes  $\Delta N_k$  in bins of constant width  $\Delta k$  to scale as  $\Delta N_k \sim k^2 \Delta k$  if the  $\mathbf{k}$  modes are uniformly distributed in three dimensions (3D). The modes  $\mathbf{k}$  have a 2D distribution for OWFA, and we expect  $\Delta N_k \sim k \Delta k$  if the modes are uniformly distributed. However, we have seen that the distribution is not uniform ( $\Delta k_{\parallel}$  and  $\Delta k_{\perp}$  have different

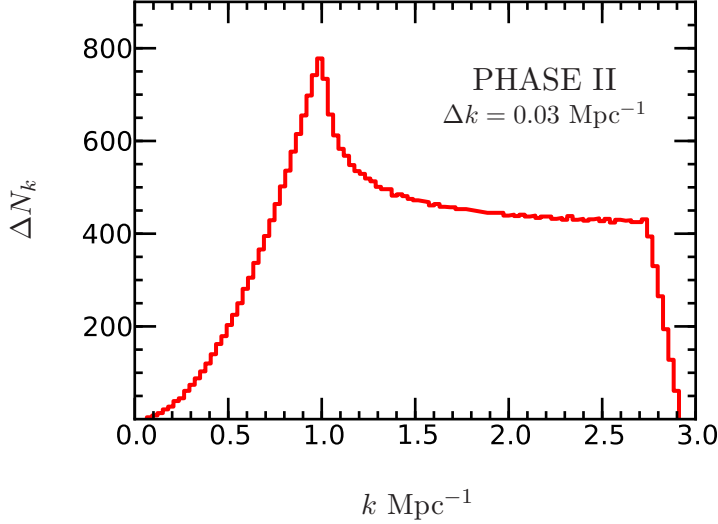


**Figure 3.** The histogram shows the number of  $k$  modes,  $\Delta N_k$  within bin width  $\Delta k$ .

values) and the histogram does not show the expected linear behaviour. The increase in  $\Delta N_k$  is faster than linear, it peaks at  $k \sim 1 \text{ Mpc}^{-1}$  and is nearly constant at  $\sim 60\%$  of the peak value for larger modes out to  $k \leq k_{\parallel}[\text{max}] \sim 3 \text{ Mpc}^{-1}$ . It is clear that a very large fraction of the Fourier modes  $k$  that will be probed by OWFA are in the range  $1 - 3 \text{ Mpc}^{-1}$ . We see that the Fourier modes all lie in this range for  $m \geq 64$  (Figure 2). The range  $k < 1 \text{ Mpc}^{-1}$  will be sampled by a relatively small fraction of the modes, and the range  $k < 0.1 \text{ Mpc}^{-1}$  will only be sampled for  $m \leq 5$ .

Figure 4 shows the diagonal and the off-diagonal elements of the signal contribution to the covariance matrix  $C_{ab}(m)$  (eq. 7). The noise contribution is also shown for reference. The noise contribution is independent of  $m$ , and it increases at the larger baselines which have a lesser redundancy  $N_A - a$ . The power spectrum  $P_{HI}(k)$  is a decreasing function of  $k$  for  $k \geq 0.1 \text{ Mpc}^{-1}$ , and most of the modes that will be probed by OWFA lie in this range. For a fixed  $m$ , the signal contribution is nearly flat for  $U < r_\nu m / (Br'_\nu)$  and then decreases if  $U$  is increased further. For  $m = 1$ , the signal at small baselines  $U \leq 10$  is comparable to the noise for  $T = 100 \text{ hr}$ . The signal is smaller than the noise at larger baselines. The overall amplitude of the signal contribution decreases for larger values of  $m$ . The signal covariance falls by a factor of  $\sim 10$  from  $m = 1$  to  $m = 8$ , and it is comparable to the noise for  $T = 1,000 \text{ hr}$ . The signal falls by another factor of  $\sim 20$  from

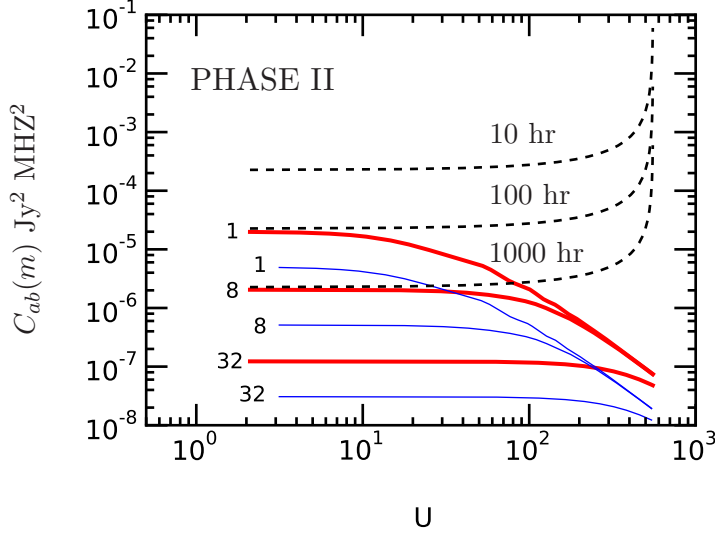


**Figure 4.** This shows the diagonal (thick red curve) and the off-diagonal (thin blue curve) elements of the signal contribution to the covariance matrix  $S_{ab}(m)$   $m = 1, 8$  and  $32$ . The system noise contribution (thick dashed black curves) to  $C_{ab}(m)$  is shown for the different observing times indicated in the figure.

$m = 8$  if we consider  $m = 32$ . We see that the HI signal is relatively more dominant at the small delay channels and the small baselines. The HI signal is considerably weaker at the larger  $m$  and  $U$ , the noise also is considerably higher at the larger baselines.

#### 4. Results

We have assumed that the HI gas, which is believed to be associated with galaxies, traces the underlying matter distribution with a constant scale independent large-scale linear HI bias  $b_{HI}$ . Incorporating redshift space distortion, we have the HI power spectrum

$$P_{HI}(\mathbf{k}) = A_{HI}^2 \bar{T}^2 [1 + \beta \mu^2]^2 P(k). \quad (15)$$

where  $P(k)$  is the matter power spectrum,  $\mu = k_{\parallel}/k$ , and

$$\bar{T}(z) = 4.66 \text{ mK} (1+z)^2 \left( \frac{\Omega_b h^2}{0.022} \right) \left( \frac{0.67}{h} \right) \left( \frac{H_0}{H(z)} \right). \quad (16)$$

The parameter  $A_{HI}$  in eq. (15) sets the overall amplitude of the HI power spectrum, and  $A_{HI} = \bar{x}_{HI} b_{HI}$  where  $\bar{x}_{HI}$  is the mean neutral hydrogen

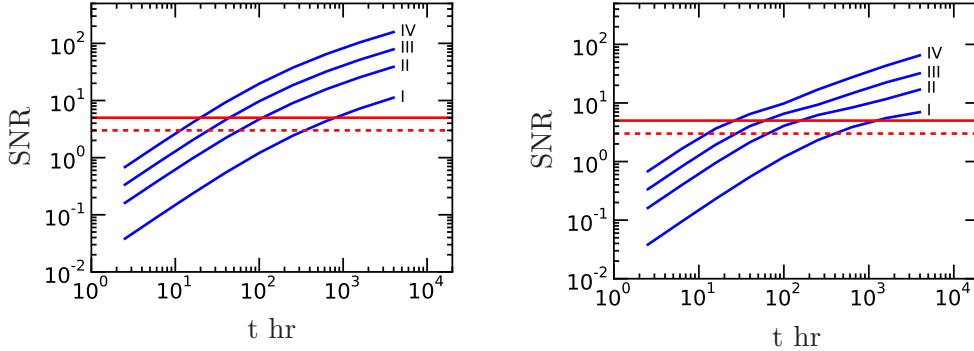


**Figure 5.** The Conditional (left) and Marginalized (right) SNR for  $A_{HI}$  as a function of the observing time for the different Phases as indicated in the figure. The horizontal dashed and solid lines show  $\text{SNR} = 3$  and  $5$  respectively.

fraction. The parameter  $\beta = f(\Omega)/b_{HI}$  is the linear redshift distortion parameter. Note that the various terms in eq. (15) are all at the redshift where the HI radiation originated, which is  $z = 3.35$  for the OWFA.

We have used the value  $\bar{x}_{HI} = 0.02$  which corresponds to  $\Omega_{gas} = 10^{-3}$  from DLA observations (Prochaska & Wolfe 2009; Noterdaeme et al. 2012; Zafar et al. 2013) in the redshift range of our interest. N-body simulations (Bagla, Khandai & Datta 2010; Guha Sarkar et al. 2012) indicate that it is reasonably well justified to assume a constant HI bias  $b_{HI} = 2$  at wave numbers  $k \leq 1 \text{ Mpc}^{-1}$ , and we have used this value for our entire analysis. This is also consistent with the Semi-empirical simulations of Marín et al. (2010). Using these values and the cosmological parameters values assumed earlier, we have  $A_{HI} = 4.0 \times 10^{-2}$  and  $\beta = 4.93 \times 10^{-1}$  which serve as the fiducial values for our analysis.

We have assumed that  $\bar{T}$  and the  $\Lambda$ CDM matter power spectrum  $P(k)$  are precisely known, and we have used the Fisher matrix analysis to determine the accuracy with which it will be possible to measure the parameters  $A_{HI}$  and  $\beta$  using OWFA observations. The Fisher matrix analysis (eq. 8) was carried out with the two parameters  $q_1 = \ln(A_{HI})$  and  $q_2 = \ln(\beta)$ .

We first focus on estimating  $A_{HI}$  the amplitude of the HI signal. The Fisher matrix element  $\sqrt{F_{11}}$  gives the signal to noise ratio (SNR) for a detection of the HI signal ( $A_{HI}$ ) provided the value of  $\beta$  is precisely known a priori (Conditional SNR). The left panel of Figure 5 shows the expected Conditional SNR as a function of the observing time, and  $t_C$  in Table 3 summarizes the time requirements for  $3 - \sigma$  and  $5 - \sigma$  detections. In reality, the value of  $\beta$  is not known a priori, and one hopes to measure this from HI

**Table 3.** Here  $t_C$  ( $t_M$ ) is the observing time required for the Conditional (Marginalized) SNR = 3 and 5 as respectively indicated in the Table.

Phase	SNR	$t_C$ (hr)	$t_M$ (hr)
Phase I	5, 3	800, 350	1190, 390
Phase II	5, 3	110, 60	150, 70
Phase III	5, 3	50, 20	50, 20
Phase IV	5, 3	20, 10	25, 15

observations. While the cosmological parameters which determine  $f(\Omega)$  are known to a relatively high level of accuracy, there is no direct observational handle on the value of  $b_{HI}$  at present. It is therefore necessary to allow for the possibility that  $b_{HI}$  can actually have a value different from  $b_{HI} = 2$  assumed here. A recent compilation of the results from several studies (Padmanabhan, Roy Choudhury & Refregier, 2014) has constrained  $b_{HI}$  to be in the range  $1.090 \leq b_{HI} \leq 2.06$  in the redshift range  $3.25 \leq z \leq 3.4$ . In our analysis we have allowed  $b_{HI}$  to have a value in a larger interval  $1.0 \leq b_{HI} \leq 3.0$ , and we have marginalized  $\beta$  over the corresponding interval  $0.329 \leq \beta \leq 0.986$ . The right panel of Figure 5 shows the expected Marginalized SNR as a function of the observing time, and  $t_M$  in Table 3 summarizes the time requirements for  $3 - \sigma$  and  $5 - \sigma$  detections.

We find (Figure 5) that for small observing times ( $t \leq 50$  hr), where the visibilities are dominated by the system noise, the Conditional and the Marginalized SNR both increase as  $\text{SNR} \propto t$ . The increase in the SNR is slower for larger observing times, and it is expected to subsequently saturate at a limiting value which is set by the cosmic variance for very large observing times not shown here. We see (Table 3) that  $\sim 1190$  hr of observation are needed for a  $5 - \sigma$  detection with Phase I. The corresponding observing time for Phase II falls drastically to 110 hr and 150 hr for the Conditional and the Marginalized cases respectively. For Phase II, the HI signal is largely dominated by the low wave numbers  $k \leq 0.2 \text{ Mpc}^{-1}$  (discussed later). Phase I which has a larger antenna spacing and smaller frequency bandwidth does not cover many of the low  $k$  modes which dominate the signal contribution for Phase II. The required observing times are  $\sim 0.5$  and  $\sim 0.25$  of those for Phase II for Phases III and IV respectively. The Marginalized SNR are somewhat smaller than the Conditional ones, the difference however is not very large. The required observing time does not differ very much except for Phase II where it increases from 110 hr to 150 hr for a  $5 - \sigma$  detection.

We have considered the joint estimation of the two parameters  $A_{HI}$  and  $\beta$  using OWFA. Figure 6 shows the expected  $1\sigma$  confidence intervals for  $\Delta\beta/\beta$  and  $\Delta A_{HI}/A_{HI}$  with three different observing times (630, 1600 and

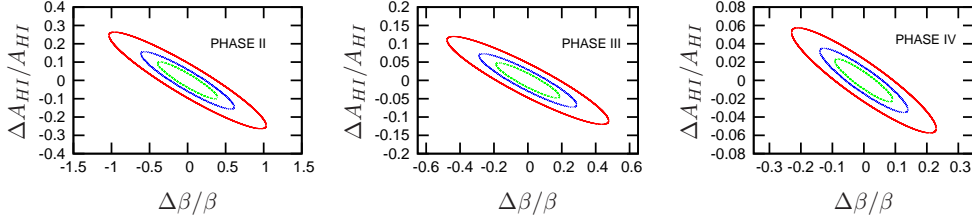


**Figure 6.** This shows the expected  $1\sigma$  contours for  $\Delta\beta/\beta$  and  $\Delta A_{HI}/A_{HI}$  with observing time 630 hrs (outer ellipses), 1600 hours (intermediate ellipses) and 4000 hours (inner ellipses) respectively for different phases indicated in the figures.

4000 hr) for Phases II, III and IV. For Phase II, a joint estimation of the parameters  $A_{HI}$  and  $\beta$  is possible with 15% and 60% errors respectively using 1600 hr of observation. The errors on the parameters  $A_{HI}$  and  $\beta$  for 4000 hr are  $\sim 2$  times smaller as compared to 1600 hr. The constraints are more tight in case of Phases III and IV. A joint detection of  $A_{HI}$  and  $\beta$  with 3% and 15% errors respectively is feasible with 1600 hr of observation with Phase IV.

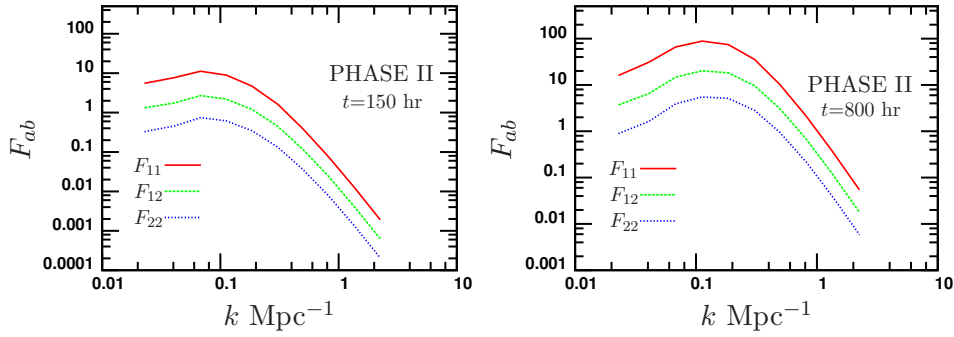


**Figure 7.** The relative contribution to the Fisher matrix components  $F_{ab}$  from the different  $k$ -modes probed by Phase II for 150 hr and 800 hr of observation respectively.

It is interesting to investigate the  $k$  range that contribute most to the HI signal at OWFA. We have seen that the Fourier modes  $k$  sampled by OWFA are predominantly in the range  $1 \leq k \leq 3 \text{ Mpc}^{-1}$ , and there are relatively few modes in the range  $k \leq 1 \text{ Mpc}^{-1}$  (Figure 3). However, the HI signal (Figure 4) is much stronger at the smaller modes, whereas the larger modes have a weaker HI signal and are dominated by the noise. It is therefore not evident

as to which  $k$  range contributes the most to the OWFA HI signal detection. Figure 7 shows the relative contributions to the Fisher matrix from the different  $k$  modes. We see that for  $t = 150$  hr, which corresponds to a  $5 - \sigma$  detection, the bulk of the contribution is from the range  $k \leq 0.1 \text{ Mpc}^{-1}$ . The larger modes do not contribute much to the signal. We have also considered  $t = 800$  hr. Here we have a slightly larger range  $k \leq 0.2 \text{ Mpc}^{-1}$  and the contribution peaks around  $k \approx 0.1 \text{ Mpc}^{-1}$ . In a nutshell, the OWFA HI signal is predominantly from the  $k$  range  $0.018 \leq k \leq 0.2 \text{ Mpc}^{-1}$ . The larger modes, though abundant, do not contribute much to the HI signal.

## 5. Summary and conclusions

We have considered four different Phases of OFWA, and studied the prospects of detecting the redshifted 21-cm HI signal at 326.5 MHz which corresponds to redshift  $z = 3.35$ . Phases I and II are currently under development and are expected to be functional in the near future. Phases III and IV are two hypothetical configurations which have been considered as possible future expansions. We have used the Fisher matrix analysis to predict the accuracy with which it will be possible to estimate the two parameters  $A_{HI}$  and  $\beta$  using OWFA. Here  $A_{HI}$  is the amplitude of the 21-cm brightness temperature power spectrum and  $\beta$  is the linear redshift space distortion parameter. For the purpose of this work we make the most optimistic assumption that the foreground contributions are not changing across different frequency channels, and hence they only contribute to the  $k_{\parallel} = 0$  mode. In reality the foreground contamination will extend to other modes also. Further, the chromatic response of the interferometer, calibration errors, systematics in the receivers and radio-frequency interference (RFI) have not been considered in the paper.

Focusing first on just detecting the HI signal, we have marginalized  $\beta$  and considered the error estimates on  $A_{HI}$  alone. We find that a  $5 - \sigma$  detection of the HI signal is possible with 1190 and 150 hr of observation for Phases I and II respectively. The observing time is reduced by factor  $\sim 0.5$  and  $\sim 0.25$  compared to Phase II for Phases III and IV respectively. We find that there is a significant improvement in the prospects of a detection using Phase II as compared to Phase I, and we have mainly considered Phase II for much of the discussion in the paper.

We have also considered the joint estimation of the parameters  $A_{HI}$  and  $\beta$ . For Phase II, a joint estimation of the parameters  $A_{HI}$  and  $\beta$  is possible with 15% and 60% errors respectively using 1600 hr of observation. To estimate  $\beta$  it is necessary to sample Fourier modes  $\mathbf{k}$  of a fixed magnitude  $k$  which are oriented at different directions to the line of sight. In other words,  $\mu = k_{\parallel}/k$  should uniformly span the entire range  $-1 \leq \mu \leq 1$ . However, the  $k_{\parallel}$  values are much larger than  $k_{\perp}$ , and the Fourier modes are largely

concentrated around  $\mu \sim 1$ , for Phase II (Section 3). The restriction arises from the limited OWFA frequency bandwidth (Table 1) which is restricted by the anti-aliasing filter.

Multi-field observations and larger bandwidth ( $> 30$  MHz) of the OWFA hold the potential to probe of the expansion history and constrain cosmological parameters using BAO measurements from the large-scale HI fluctuations at  $z = 3.35$ . Anisotropies in the clustering pattern in redshifted 21-cm maps at this redshift produced by Alcock-Paczyski effect has the possibility of probing cosmology and structure formation. It is also possible to constrain neutrino masses of using OWFA and compare among different fields of cosmology (LSS, CMBR, BBN). Thus the OWFA could provide highly complementary constraints on neutrino masses. We leave investigation of such issues for future studies.

The present work has assumed that the shape of the HI power spectrum is exactly determined by the  $\Lambda$ CDM model, and has only focused estimating the overall amplitude  $A_{HI}$  from OWFA observations. The OWFA HI signal is predominantly from the  $k$  range  $0.02 \leq k \leq 0.2 \text{ Mpc}^{-1}$ . It is possible to use OWFA observations to estimate  $P_{HI}(k)$  in several separate bins over this  $k$  range, without assuming the anything about the shape of the HI power spectrum. In a forthcoming paper, we plan to calculate Fisher matrix estimates for the binned power spectrum.

## Acknowledgment

The authors acknowledge Jayaram N. Chengalur, Jasjeet S. Bagla, Tirthankar Roy Choudhury, C.R. Subrahmanya, P.K. Manoharan and Visweshwar Ram Marthi for useful discussions. AKS would like to acknowledge Rajesh Mondal and Suman Chatterjee for their help. SSA would like to acknowledge CTS, IIT Kharagpur for the use of its facilities and the support by DST, India, under Project No. SR/FTP/PS-088/2010. SSA would also like to thank the authorities of IUCAA, Pune, India for providing the Visiting Associateship programme.

## References

- Ali, S. S., Bharadwaj, S. 2014, *Journal of Astrophysics and Astronomy*, 35, 157
- Ali, S. S., Bharadwaj, S., & Pandey, S. K. 2006, *MNRAS*, 366, 213
- Ade, P. A. R., Aghanim, N., et al. *A&A* 571, A16 (2014)
- Ansari, R., Campagne, J. E., Colom, P., et al. 2012, *A & A*, 540, A129
- Bagla J. S., Khandai N., Datta K. K., 2010, *MNRAS*, 407, 567
- Bandura, K., Addison, G. E., Amiri, M., et al. 2014, arXiv:1406.2288
- Bharadwaj, S., Nath, B., Sethi, S. K., 2001, *JApA*, 22, 21
- Bharadwaj, S., Sethi, S. K., 2001, *JApA*, 22, 293
- Bharadwaj S., Pandey S. K., 2003, *JApA*, 24, 23



- Bharadwaj, S., & Srikant, P. S. 2004, JApA, 25, 67  
Bharadwaj S., Ali S. S., 2005, MNRAS, 356, 1519  
Bharadwaj S., Sethi S., Saini T. D., 2009, Phys Rev. D, 79, 083538  
Bull et al. 2015, ApJ, 803, 21  
Chang, T.-C., Pen, U.-L., Peterson, J. B., McDonald, P., 2008, Phys Rev. Lett., 100, 091303  
Eisenstein D. J., Hu W., 1998, ApJ, 496, 605  
Ghosh, A., Bharadwaj, S., Ali, S. S., & Chengalur, J. N. 2011a, MNRAS, 411, 2426  
Ghosh, A., Bharadwaj, S., Ali, S. S., & Chengalur, J. N. 2011b, MNRAS, 418, 2584  
Guha Sarkar, T., Mitra, S., Majumdar, S., Choudhury, T. R., 2012, MNRAS, 421, 3570  
Guha Sarkar, T., & Hazra, D. K. 2013, JCAP, 4, 2  
Marin F. A., Gnedin, N. Y., Seo, H.-J., Vallinotto, A. 2010, Ap.J, 718, 972  
Mao, X.-C. 2012, Ap.J, 744, 29  
Morales, M. F. 2005, ApJ, 619, 678  
Noterdaeme, P., Petitjean, P., Carithers, W. C., et al. 2012, A & A, 547, L1  
Padmanabhan, H., Roy Choudhury, T., Refregier, A., MNRAS, 447, 3745-3755 (2015)  
Prasad, P., Subrahmanya, C. R. 2011a, arXiv:1102.0148.  
Prasad, P., Subrahmanya, C. R. 2011b, Experimental Astronomy, 31, 1  
Prochaska, J. X., Wolfe, A. M. 2009, ApJ, 696, 1543  
Ram Marthi, V., Chengalur, J., 2014, MNRAS, 437 (1), 524  
Sarma, N. V. G., Joshi, M. N., Bagri, D. S., Ananthakrishnan, S. 1975, J. Instn Electronics Telecommun. Engr., 21, 110.  
Seo, H.-J., Dodelson, S., Marriner, J., et al. 2010, ApJ, 721, 164  
Swarup, G., Sarma, N. V. G., Joshi, M. N., Kapahi, V. K., Bagri, D. S., Damle, S. H., Ananthakrishnan, S., Balasubramanian, V., Bhave, S. S., Sinha, R. P. 1971, Nature Phys. Sci., 230, 185.  
Villaescusa-Navarro, F., Viel, M., Datta, K. K., & Choudhury, T. R. 2014, JCAP, 9, 050  
Visbal, E., Loeb, A., Wyithe, S., 2009, JCAP, 10, 30  
Wyithe, J. S. B., & Loeb, A. 2009, MNRAS, 397, 1926  
Zafar, T., Péroux, C., Popping, A., et al. 2013, A & A, 556, A141